Annals of Biomedical Engineering, Vol. 45, No. 11, November 2017 (© 2017) pp. 2524–2534
DOI: 10.1007/s10439-017-1889-2

A Comprehensive Characterization of Parameters Affecting High-Frequency Irreversible Electroporation Lesions

TYLER MIKLOVIC,[1] EDUARDO L. LATOUCHE,[1] MATTHEW R. DEWITT,[1] RAFAEL V. DAVALOS,[1] and MICHAEL B. SANO[2,3]

[1]Virginia Tech-Wake Forest School of Biomedical Engineering and Sciences, Blacksburg, VA, USA; [2]Department of Radiation Oncology, Stanford University School of Medicine, Stanford, CA, USA; and [3]UNC-NCSU Joint Department of Biomedical Engineering, Chapel Hill, NC, USA

(*Received 13 April 2017; accepted 12 July 2017; published online 18 July 2017*)

Associate Editor Leonidas D. Iasemidis oversaw the review of this article.

Abstract—Several focal therapies are being investigated clinically to treat tumors in which surgery is contraindicated. Many of these ablation techniques, such as radiofrequency ablation and microwave ablation, rely on thermal damage mechanisms which can put critical nerves or vasculature at risk. Irreversible electroporation (IRE) is a minimally invasive, non-thermal technique to destroy tumors. A series of short electric pulses create nanoscale defects in the cell membrane, eventually leading to cell death. Typical IRE protocols deliver a series of 50–100 μs monopolar pulses. High frequency IRE (H-FIRE) aims to replace these monopolar pulses with integrated bursts of 0.25–10 μs bipolar pulses. Here, we examine ablations created using a broad array of IRE and H-FIRE protocols in a potato tissue phantom model. Our results show that H-FIRE pulses require a higher energy dose to create equivalent lesions to standard IRE treatment protocols. We show that ablations in potato do not increase when more than 40 H-FIRE bursts are delivered. These results show that H-FIRE treatment protocols can be optimized to produce clinically relevant lesions while maintaining the benefits of a non-thermal ablation technique.

Keywords—Focal ablation, Non-thermal therapy, H-FIRE, Tissue phantom.

INTRODUCTION

Electroporation is a phenomenon that takes place when cells are exposed to intense electric fields, which dramatically change the transmembrane potential and lead to the creation of nanopores on the cell membrane.[1,2] In clinical settings, non-lethal pulses have been administered to increase the permeability of cell membranes, allowing for the passage of large macromolecules through the membrane of targeted cells. These treatment modalities are referred to as electrochemotherapy[3,4] or electro-gene therapy,[1,2,5,6] depending on the adjunctive macromolecule. These therapies aim to minimize the lethality of the electrical pulses to optimize the biological effect of the injected therapy. In contrast, irreversible electroporation (IRE) protocols are designed to permanently disrupt cell membranes within a targeted region.[7,8] IRE mechanisms are independent of thermal processes and clinical protocols are designed to minimize temperature rises in the tissue. This makes IRE an ideal treatment option for tumors near critical blood vessels and nerves where thermal ablative techniques, including radiofrequency and microwave ablation, may cause collateral damage or may be limited by the heat-sink effect.[9,10] Recent clinical trials have demonstrated that IRE is highly efficacious for tumors where surgical removal or thermal ablation are contraindicated.[11]

Clinically, IRE is accomplished via introduction of percutaneous needle electrodes into or around the target tissue and a series of high voltage pulses, ranging from 50 to 100 μs in duration, are delivered.[11–13] Typical IRE protocols deliver 80–100 pulses, each separated by an approximately 1 s delay. When implemented clinically, pulses are synchronized with the patient's heartbeat to minimize triggering of irregular heartbeats and a robust anesthetic protocol including a neuromuscular blockade is implemented to prevent the stimulation of muscle contractions.[14] The NanoKnife clinical ablation system (AngioDynamics, Inc., Latham, NY) utilizes a voltage-to-distance ratio

Address correspondence to Michael B. Sano, UNC-NCSU Joint Department of Biomedical Engineering, Chapel Hill, NC, USA. Electronic mail: mikesano@med.unc.edu

of 1500–1700 V/cm and the output voltage is adjusted based on physician-reported measurements of electrode spacing.[15]

A positive review highlighting the safety and efficacy of these treatments in a clinical setting was recently published by Scheffer *et al.*[16] and IRE appears to be ideally suited for the treatment of tumors less than 3 cm in each dimension with a success rate between 93%[17] and 98%.[18] IRE is currently being evaluated as a treatment modality against a number of oncological disorders including pancreatic,[15,19,20] lung,[21] brain,[22] kidney,[23–27] and liver[28,29] cancers. Long-term follow-up on these patients indicated that IRE has the potential to leave critical blood vessels, nerves, and the more general healthy stroma unharmed.[30–32]

While the past decade is marked by numerous positive results from IRE trials, a prospective clinical trial for lung tumor treatment was stopped when investigators observed that only 30% of treatment subjects ($n = 7$) showed complete tumor regression at the 12-month follow-up.[33] The reason for this inconsistency is unclear; however, it is potentially due to the large degree of heterogeneity in lung tissue. The presence of air pockets may also insulate and/or protect regions of the tumor, possibly diminishing the overall effectiveness of standard IRE treatments.[34] The complexity of treating tumors in these highly heterogeneous tissues and the need to administer a neuromuscular paralytic to avoid intense muscle contractions apparent in standard IRE treatments necessitate the research and development of novel IRE pulse protocols to mitigate these challenges.

High frequency IRE (H-FIRE) is a relatively new variant of IRE which replaces monopolar 100 μs pulses with a burst of shorter duration (0.25–5.0 μs) alternating positive and negative (bipolar) pulses separated by a short inter-pulse delay (Fig. 1). Theoretical models of H-FIRE predict that this therapy is capable of penetrating heterogeneous tissues and producing more predictable ablations than typical IRE pulses.[35] For example, blood vessels in the treatment area can influence the electrical field of standard IRE pulses if they are not properly accounted for.[36] This is due to the fact that IRE pulses are relatively long in duration ($\geq$50 μs) and therefore have lower frequency components ($<$20 kHz), which are susceptible to the effects of heterogeneity (Supplemental Fig. 1a). At these frequencies, the impedance of muscle, fat, stroma, and other tissues can vary significantly from healthy or tumorous tissue.[37] At higher frequencies the differences in impedance between these tissue types are minimized (Supplemental Fig. 1b) and the tissue appears more electrically homogeneous and therefore an electric field distribution which more closely matches the analytical solution is produced.[38] Arena *et al.* recently demonstrated that bursts of 1 or 2 μs pulses can be used to ablate tissue while additionally eliminating the muscle contractions associated with IRE pulses, further contributing to the efficacy and potential of H-FIRE in the tumor ablation field.[39] Siddiqui *et al.* recently showed that H-FIRE can be safely and predictably delivered next to critical hepatic anatomy such as vascular and biliary structure.[10]

H-FIRE pulses are situated in a relatively unexplored region of the pulse-duration space[40] and the lethal electric field thresholds and long term biological responses for these pulse waveforms are comparatively unknown. The transmembrane potential does not rise instantaneously during exposure to a pulsed electric fields[41] and the charging time for mammalian cell membranes is approximately 1 μs.[42] As result, a number of interesting biological response arise when H-FIRE pulses are delivered. The processes of pore formation and expansion appear to decrease for short pulse durations (0.25–5 μs) as compared to longer duration pulses in the 100 μs to 10 ms range and permeabilization of the cell membrane may not be as robust or long lasting for short pulses.[43]

Current H-FIRE protocols mimic clinical IRE delivery procedure by energizing each burst for 50–100 μs and applying a series of 80–100 bursts at a 1 Hz repetition rate. Recent studies have shown that the lethal electric field threshold increases significantly as pulse duration is decreased.[41] An H-FIRE protocol consisting of 80 bursts of 1–5 μs pulses was shown to reduce the viability of pancreatic cancer cells in suspension to less than 20% for fields strengths of 3000 V/cm or more. In contrast, it was shown that 1250 V/cm is for equivalent energy 100 μs IRE protocols to reduce the viability of these cells to the same extent.[44] For cells in suspension, H-FIRE protocols utilizing 250 and 500 ns pulses appear to be relatively ineffective even at field strengths up to 4000 V/cm. However, when cells are grown in collagen tumor mimics, lethal thresholds of 2000, 1700, 1100, 760 V/cm were found for H-FIRE protocols with 0.25, 0.5, 1.0, and 2.0 μs pulses, respectively.[45] Similar studies found that IRE protocols had a lethal threshold of 500 V/cm in collagen tumor mimics[44] and 300–640 V/cm in liver tissue.[46–48] This discrepancy between cells in suspension, those grown in a physiologically mimicking environment, and *in vivo* highlights the need for further investigation of these novel protocols and their resulting thresholds.

In this work, potato tissue phantoms are used as a surrogate to enable the testing of a wide parameter array including the number of bursts and individual pulse duration in search of a potentially optimized treatment protocol. We investigated the lesion volumes produced by a clinical prototype system which can deliver bipolar H-FIRE pulses up to 2500 V in

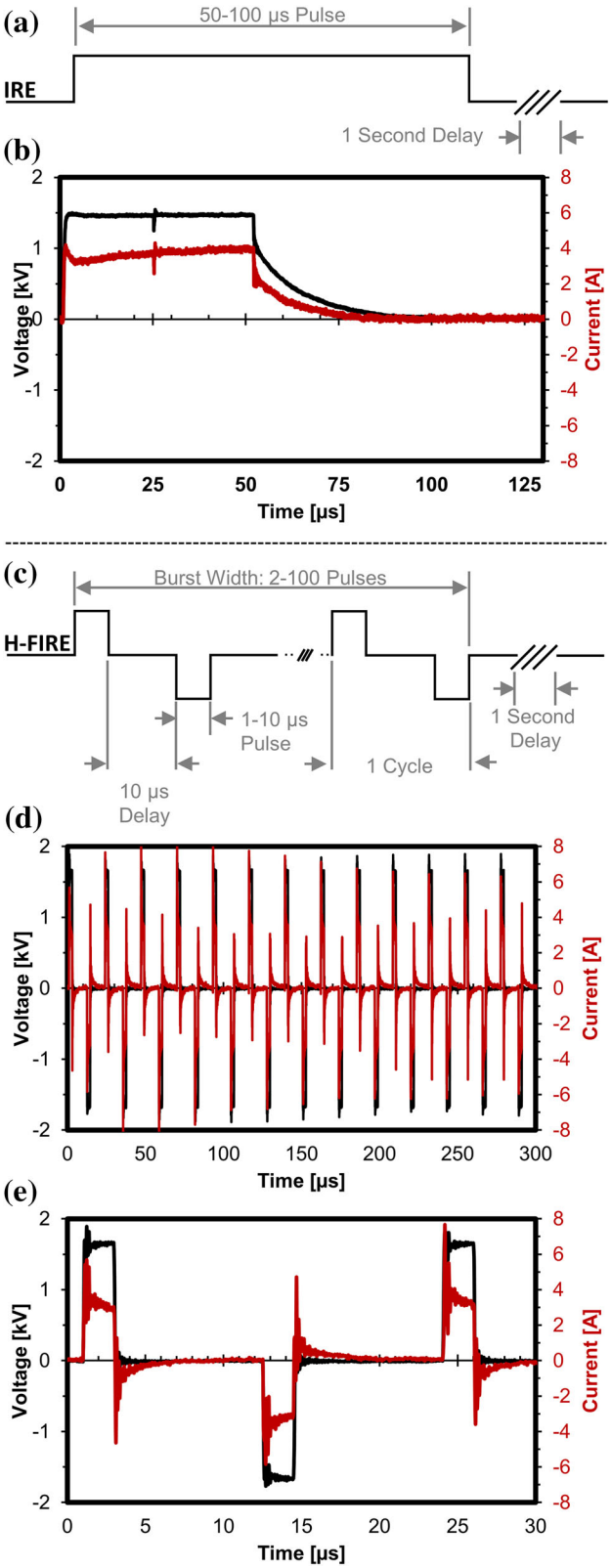

FIGURE 1. H-FIRE protocols replace the monopolar IRE pulses with a burst of bi-polar pulses. (a) Standard IRE protocol delivers 50–100 µs mono-polar pulses separated by a 1 s inter-pulse delay; (b) experimental 1.5 kV 50 µs IRE pulse; (c) H-FIRE protocols deliver a high frequency burst of 1–10 µs bi-polar pulses. Each burst of pulse cycles is separated by a 1 s delay. Energized time per burst or dose rate, represents the total charged time per burst; (d) experimental 1.5 kV H-FIRE burst with 26 × 2 µs pulses and a 10 µs delay between alternating polarity pulses; and (e) the first three alternating pulses within an H-FIRE burst.

amplitude. We show that when delivering the same amount of energy, there is a logarithmic relationship between pulse width (*PW*) and ablation size. Finally, we show that there is no statistical difference in the ablation volumes created by delivering 40 through 200 bursts across two needle electrodes. This work highlights the need to understand the effect of unique parameters associated with H-FIRE not present in IRE to result in clinically useful application of H-FIRE for tissue ablation.

MATERIALS AND METHODS

Electroporation Setup

Experiments were performed using potatoes as a tissue phantom to enable the evaluation of a large number of parameters. Potato tissue is relatively homogeneous and exhibits a significant increase in conductivity after electroporation, mimicking the response seen *in vivo*.[2,49] While potato does not recapitulate all of the properties of an *in vivo* tumor, it is a reasonable model for assessing trends and enables comparison of ablations to numerical models to determine the lethal thresholds as is done *in vivo*.[47,50,51] Lesions created in the tissue become visible 12–24 h post treatment due to the production of melanin[52] and are easily measured using calipers.

Monopolar IRE pulses were generated using a commercial pulse generator (ECM 830, Harvard Apparatus, Holliston, MA) and bipolar H-FIRE pulses were generated using a custom pulse generator. Treatments were delivered to the tissue through two 1.0 mm diameter clinical IRE probes (*NanoKnife*™ Single Electrode Probes, AngioDynamics, Inc., Latham, NY) separated by 1.0 or 2.0 cm. These probes have an adjustable polyimide sheath which was retracted to expose 0.5 cm of the stainless steel electrodes. Voltage and current measurements were recorded using a custom high speed data acquisition system. To facilitate comparison between groups, a simplified electrical dose formula was used

$$Dose = V^2 * T_p * n * N\ (\mathrm{V^2\ s}), \qquad (1)$$

where V is the applied voltage, T_p is the *pulse width*, n is the number of pulses per burst, and N is the number of bursts per treatment. This calculation of dose was

TABLE 1. Treatment protocols evaluated.

Voltage (V)	Pulse width (μs)	Delay (μs)	# of bursts	On-time per burst (μs)	Energy dose (V^2 s)	Lesion volume (cm^3)
1500	1	10	100	50	11,250	1.8
1500	2	10	100	50	11,250	3.1
1500	5	10	100	50	11,250	5.6
1500	50	10	100	50	11,250	12.6
2000	2	10	10	100	4000	1.8
2000	2	10	20	100	8000	5.7
2000	2	10	40	100	16,000	7.2
2000	2	10	60	100	24,000	8.1
2000	2	10	80	100	32,000	8.2
2000	2	10	100	100	40,000	8.1
2000	2	10	150	100	60,000	9.5
2000	2	10	200	100	80,000	8.5

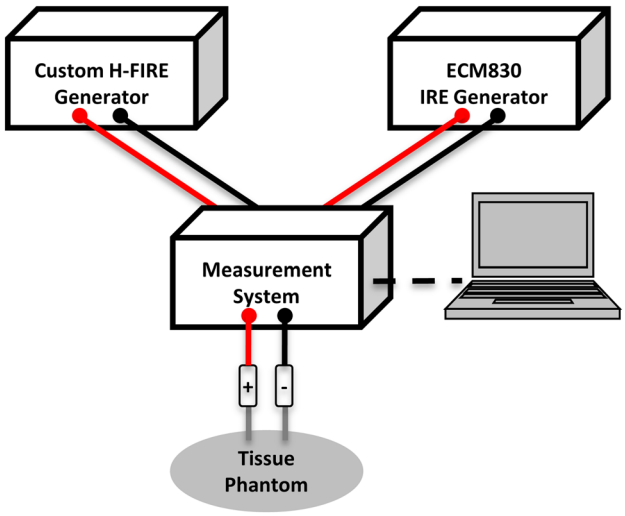

FIGURE 2. Experimental set-up. A custom pulse generator produces bipolar H-FIRE pulses (top left). The BTX ECM 830 pulse generator produces standard monopolar IRE pulses (top right). A custom measurement system (center) records the pulses and displays voltage, current, and resistance data on a laptop computer.

chosen as a simple way to compare the ablation outcomes between treatments with varied pulse parameters. It was recently shown by Sano *et al.* that when only voltage is varied between H-FIRE treatments, this calculation of equivalent dose results in equivalent lethal thresholds.[45] Here, we compare treatments where voltage is held constant and other parameters are varied.

Pulse parameters used during this study are shown in Table 1 and the experimental set-up is shown in Fig. 2. 48 h post-treatment, the potatoes were sliced parallel to the electrode paths to expose the ablated region. Lesions were compared by measuring the optically visible lesions in potato tissue, which became distinctively darker in color, 48 h post-treatment.

The visibly darkened tissue is the result of the oxidation process catalyzed by polyphenol oxidase released as the cell membranes lose integrity resulting in the generation of melanins.[52,53] In a preliminary study, potatoes were sectioned incrementally between 6 and 72 h post-treatment and 48 h was determined to be the optimal time post-treatment for full coloration of the ablation zone to occur. Additionally, potatoes were sectioned at 30 h and the boundary of the ablation was monitored for 6 h. Over this time, the ablation volume remained constant (Supplemental Fig. 2), indicating that melanins were not diffusing out into untreated regions and confounding measurements. The characteristic lesion resulting from electroporation treatment displays a near-ellipsoid shape and lesion volume was calculated by representing the lesion as an ellipsoid with volume (v)

$$v = \frac{4}{3} \cdot \pi \cdot a \cdot b \cdot c \ [\mathrm{cm}^3], \tag{2}$$

where a, b, and c are one half of the length, width, and depth of the ablations. All values are reported as mean ± standard deviation.

Finite Element Analysis

In silico models for determining the lethal thresholds of IRE and H-FIRE treatments were generated using COMSOL Multiphysics (V4.3, COMSOL, Palo Alto, CA). The general geometry of the potato tissue was represented as an ellipsoid with the average dimensions of the tissue phantoms. Two 0.5 cm long cylindrical geometries with a 1 mm diameter were inserted into the center of the domain to mimic the experimental placement of the electrodes. The electric field distribution was found by solving the equation:

$$\nabla \cdot (\sigma_d \nabla \varphi) = 0 \ [\mathrm{A/m}^3], \tag{3}$$

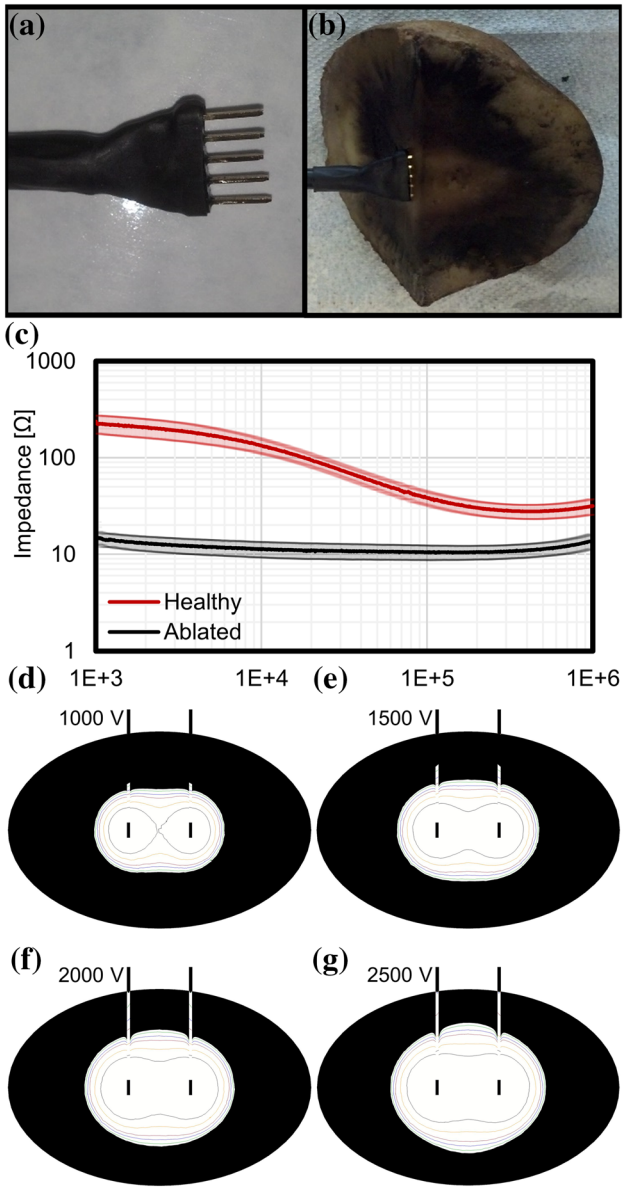

FIGURE 3. Electrical impedance spectrum of potato tissue before and after ablation. (a) A five electrode impedance probe was used to (b) measure the electrical impedance of ablated and untreated regions of the tissue between 1 kHz and 1 MHz; (c) there is a significant difference in the conductivity of healthy and ablated tissue at all frequencies in this range. A maximum difference of 13.9× was observed at 1 kHz and a minimum difference of 2.3× was observed at 1 MHz; and (d–g) numerical simulations showing the 125 V/cm iso-contours for models using 1×, 2×, 4×, 6×, 10×, and 15× changes in conductivity (inside to outside). Simulations were conducted with (d) 1.0 kV; (e) 1.5 kV; (f) 2.0 kV; and (g) 2.5 kV between the electrode pairs.

where σ_d represents the electrical conductivity of the tissue as a function of the applied electric field and φ is the electric potential.[54] Boundary values for the electrode–tissue interface were set to $\varphi = V_0$ and 0, where V_0 is the experimental voltage. A sigmoidal changing conductivity function was incorporated into the model to simulate the changes due to electroporation by implementing a piecewise function in COMSOL which was smoothed to be second derivative continuous with a center point at 255 V/cm, the approximate IRE threshold of potato tissue.[55] The initial conductivity of 0.039 S/m was chosen based on experimental measurements.

It was found that the conductivity of healthy untreated tissue was significantly higher than tissue within the experimental ablation zones (Fig. 3). Additionally, this change in conductivity was frequency dependent with a larger change occurring at 1 kHz than at 1 MHz. To account for these changes, the simulations were repeated for multiple values of conductivity change. The maximum conductivity used in the sigmoidal function set as a multiple (1×–15×) of the initial conductivity based on impedance measurements of healthy and ablated tissue (Fig. 3). Multipliers of 2×, 2×, 3×, and 9× were used for the 1, 2, 5, and 50 μs pulse duration groups, respectively. These values reflect the change in impedance between healthy and ablated tissue measured at 1 MHz, 500 kHz, 200 kHz, and 20 kHz, respectively and correspond to the center frequency of each pulse group. Multiplier values were rounded to the nearest integer. All remaining boundaries were defined as electrically insulating.

$$\mathbf{n} \cdot \mathbf{J} = 0 \ [\mathrm{A/m^2}], \tag{4}$$

where $\mathbf{n}$ is the normal vector to the surface, $\mathbf{J}$ is the electrical current density.

To improve the simulations, two strategies were employed. First, a two-step simulation was conducted where a stationary 'pre-pulse' was applied using a voltage of 50 V. This voltage does not result in electric fields sufficiently high enough to change the tissue conductivity and allows the simulation to determine a baseline electric field distribution. The solution to this simulation was used as the initial values of a second sequential stationary solver with the experimental voltage applied to the energized electrode. This process significantly reduces the simulation time. Second, the relative tolerance of each of these solvers was reduced from the default of 0.01 to 1E−12. The nonlinear method was changed from automatic (Newton) to automatic highly nonlinear (Newton) with a maximum number of iterations of 2500, an initial damping factor of 1E−8, and minimum damping factor of 1E−16. This forces the solver to search for a more accurate solution and eliminates finite element artifacts.

The electrodes were given a default 'extra fine' mesh and the main simulation geometry was defined as a 'normal' mesh. This mesh was refined once and the maximum error between additional successive refine-

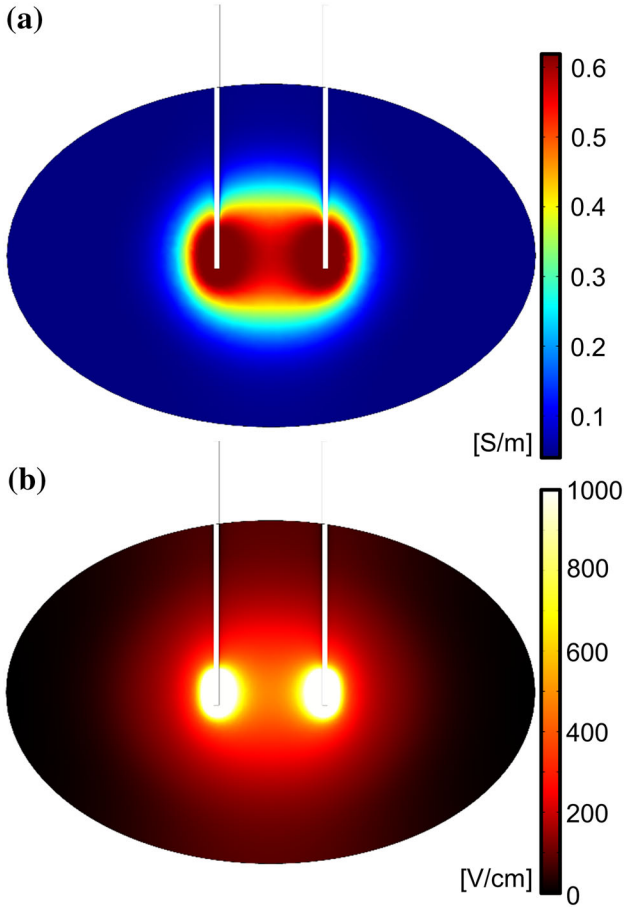

FIGURE 4. Finite element modeling of tissue phantom to determine lethal thresholds. (a) A dynamic conductivity map was used to model the instantaneous effects of electroporation on the tissue's electrical properties; and (b) electric field distribution when 2500 V was applied between the two energized electrodes.

ments was 1.8% and the average error was 0.3%. The simulation solved 867,257 degrees of freedom using a mesh with 636,893 domain elements, 39,994 boundary elements, and 3122 edge elements. The simulations for all voltage and conductivity values were completed in approximately 145 h on an Intel i7 quad core processor with 32 GB RAM. Results of these simulations with 2500 V applied between the electrodes are shown in Fig. 4.

Determination of Electric Field Threshold for Cell Death

48 h post-electroporation, the measured width, height, and depth of the darkened region of the potato tissue were recorded (Supplemental Fig. 3). These measurements were matched to an electric field magnitude in the x, y, and z axis obtained from the finite element analysis. All experimental groups reported were repeated a minimum of three times ($N = 3$) and

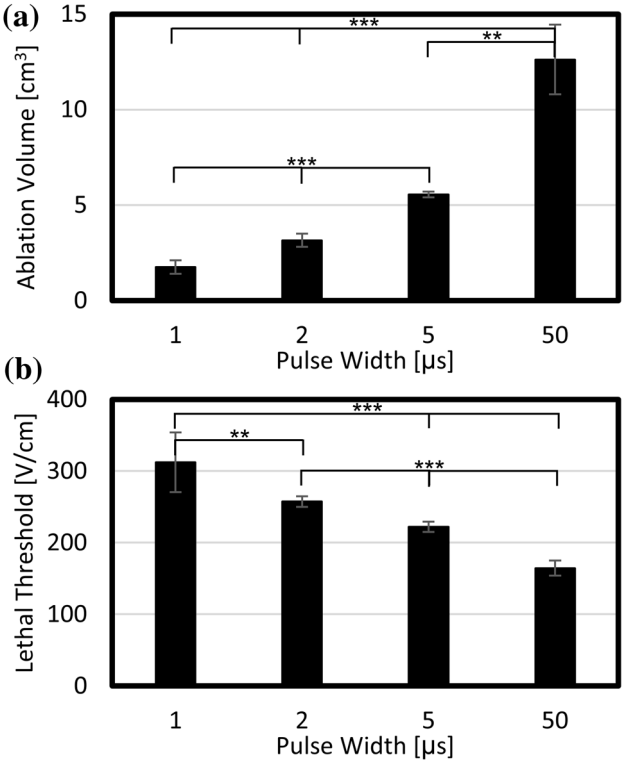

FIGURE 5. Constitutive pulse length has a large effect on lesion volumes when treatments deliver equivalent energy doses. Bursts with shorter constitutive pulses produced smaller ablations. The data shows a strong logarithmic correlation ($y = 2.81 * \ln(x) + 1.38$) between pulse length and lesion volume (r^2 value of 0.995). All values between groups were found to be statistically significantly different for $\alpha = 0.05$ (**) and $\alpha = 0.01$ (***).

the mean ± standard deviation for each group were determined from the electric field strengths determined in all three dimensions (e.g., a minimum of nine values).

RESULTS

Equivalent Energy: Pulse Width Analysis

To investigate the effects of constituent *PW*s on lesion volume, four treatment groups receiving equivalent energy doses with varying *PW*s were investigated. Electrical dose was held constant at 11,250 V^2 s by energizing the electrodes to 1500 V and delivering 100 bursts, each energized for 50 μs. Bursts with 1, 2, and 5 μs bipolar pulses or 50 μs monopolar constitutive pulses were evaluated with 50, 24, 10, and 1 pulses per burst, respectively. This method for defining dose was based on the assumption that H-FIRE treatments will be constrained to the on-time (50–100 μs) and pulse repetition rates (1 Hz or cardiac synchronization) currently employed in the clinic.

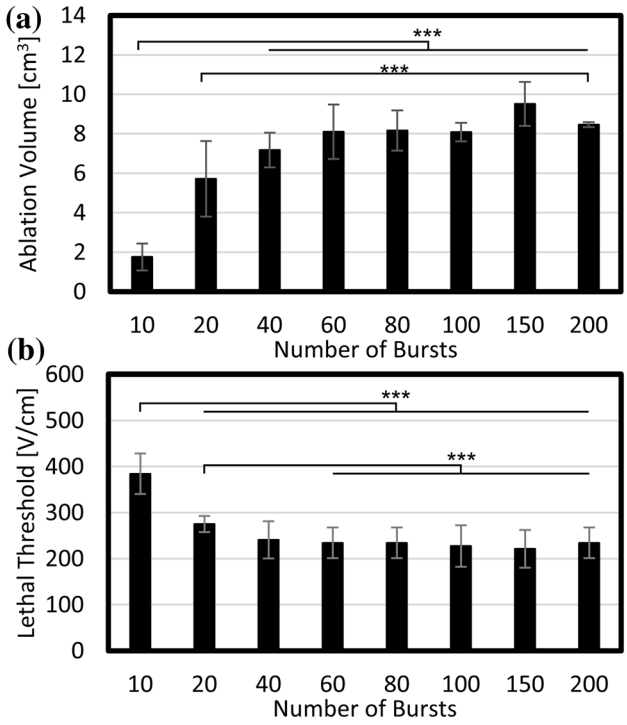

FIGURE 6. Ablations created with bursts of 2 μs pulses where each burst was energized for 100 μs. (a) Treatments with 10× bursts produced the smallest ablation volumes. Ablation volumes increased sequentially when 20×, 40×, and 60× bursts were delivered. However, no significant increases in ablation volume were found for trials where 60 pulses or more were administered; and (b) the lethal threshold decreased sequentially when 10×–60× bursts were delivered. However, no significant changes in lethal threshold were found between treatments receiving 40 or more bursts. Statistical significance between groups was determined using a one-sided Student's *T* test with unequal variances and $\alpha = 0.01$ (***).

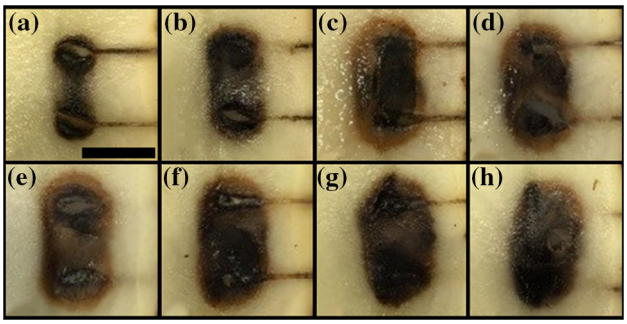

FIGURE 7. Ablations created with a 2 cm separation, 0.5 cm exposure, 2500 V amplitude pulses. (a) 10×; (b) 20×; (c) 40×; (d) 60×; (e) 80×; (f) 100×; (g) 150×; and (h) 200× bursts. Delivery of more than 40 bursts does not significantly increase lesion volume. Scale bar is 2 cm.

We found that lesion volumes increased as constituent pulse duration increased despite delivering equivalent doses of integrated energy (Fig. 5a). Bursts with 1, 2, 5, and 50 μs pulses produced lesion volumes with the following means and standard deviations: 1.75 ± 0.36, 3.14 ± 0.34, 5.56 ± 0.15, and 12.57 ± 1.82 cm^3, respectively. The lethal threshold for these same respective groups were 312.3 ± 41.8, 257.3 ± 7.6, 222.0 ± 7.0, and 164.4 ± 10.4 V/cm (Fig. 5b). The lethal thresholds and ablation volumes were found to be statistically significantly different between all groups ($\alpha \leq 0.05$).

Burst Number Analysis on Lethal Thresholds

Typical IRE protocols prescribe the delivery of 80–100 pulses. To investigate how deviating from this affects the treatment volume, we investigated six additional protocols. The number of bursts was varied between 10 and 200. Applied voltage (2000 V), *PW* of (2 μs), and an energized time of per burst (100 μs) were held constant. This enabled the electrical dose to vary between 4000 and 80,000 V^2 s. A higher voltage was used in this experiment to ensure that the 10× burst group produced contiguous lesions.

The data shown in Fig. 6, indicates that lesion volume increases between 10 and 40 bursts. Treatment volume plateaued for groups that received more than 40 bursts. Treatments with 10, 20, 40, 60, 80, 100, 150, and 200 bursts produced lesions which were 1.76 ± 0.68, 5.72 ± 1.91, 7.17 ± 0.87, 8.10 ± 1.38, 8.16 ± 1.01, 8.08 ± 0.47, 9.52 ± 1.12, 8.46 ± 0.13 cm^3, respectively. The lethal threshold for these same respective groups were 417.8 ± 44.8, 301.5 ± 40.1, 268.7 ± 39.1, 261.8 ± 39.5, 258.4 ± 40.1, 256.0 ± 48.5, 246.6 ± 42.1, and 258.6 ± 32.8 V/cm. Representative ablations from these groups can be seen in Fig. 7. The ablation volumes for treatments with 10 bursts displayed statistically significantly differences compared to groups receiving 40–200 bursts ($\alpha = 0.01$). The ablation volume created by 20 bursts was also statistically different from the volume created by 200 bursts ($\alpha = 0.01$). The lethal thresholds for treatments with 10 bursts were statistically different than all groups ($\alpha = 0.01$) and treatments receiving 20 bursts had statistically different thresholds than the groups receiving 60 or more bursts. The lethal thresholds for groups with 40 through 200 bursts were not found to be statistically significantly different.

DISCUSSION

H-FIRE is a relatively new tissue ablation technique and the effects of different protocols on resulting lesion volume have not been fully examined. When investigating the effects of *PW*, it was found that when electrical dose is held constant, bursts with longer pulses are significantly more effective at ablating tissue.

Bursts with 50 μs constitutive pulses produced lesion volumes which were 7.2× larger than those with 1 μs constitutive pulses. This trend was highly correlated to a logarithmic curve [$volume = 1.28 \cdot \ln(PW) + 1.38$ (cm^3), $r^2 = 0.995$], where PW is the pulse width in μs.

The lethal threshold found for H-FIRE protocols with 50 μs bursts (Fig. 5b) was approximately 165 V/cm in our potato tissue phantom. Similar IRE protocols in liver and brain suggest a lethal threshold of approximately 500 V/cm for mammalian tissue,[22,46] 3× greater than the potato tissue phantom. We anticipate that H-FIRE protocols will follow a similar trend *in vivo* and require an electric field approximately three times greater than potato to ablate mammalian tissue. Here we found lethal thresholds of 257 and 227 V/cm for 2 μs H-FIRE protocols with 100 bursts which were energized for 50 and 100 μs, respectively. Applying this 3× assumption, these protocols should require approximately 680–770 V/cm to ablate mammalian tissue. Lethal thresholds for pancreatic cancer cells grown in 3D culture were found to be 855 and 718 V/cm for H-FIRE treatments with 2 μs constitutive pulses energized for 50 and 100 μs, respectively.[45] Similar 2 μs H-FIRE treatment protocols delivered to *in vivo* rabbit liver corresponded to a lethal threshold of 861 V/cm which were 2.5–2.7× higher than matched 50 and 100 μs IRE treatments, respectively.[56] This indicates that ablations in potato tissue can provide some limited guidance for the development of clinical protocols.

While longer duration pulses appear to be more effective at ablating tissue, muscle contraction intensity is highly correlated to pulse duration. In clinical settings, 50–100 μs pulse lengths require a very intense anesthetic protocol to minimize these muscle contractions[14] and delivery with cardiac synchronization in order to avoid inducing arrhythmia.[57] A critical advantage of the H-FIRE protocol is the use of ultrashort bipolar pulses which have the potential to eliminate these muscle contractions. Rogers *et al.* showed that the threshold for muscle contractions, of gastrocnemius muscles, increased from 1.83 to 112 V/cm when pulse duration was decreased from 100 to 1 μs, a 61× increase. In practical terms, this means that a significantly smaller volume of tissue will be exposed to muscle stimulating electric fields when 1 μs pulses are applied (Supplemental Fig. 4). In contrast, we show here that the lethal threshold for bursts of 1 μs pulses is only 1.9× higher than for mono-polar 50 μs pulses. The significant increase in muscle contraction threshold paired with a relatively small increase in lethal threshold indicates that clinically relevant ablations can be created without inducing the extreme muscle contractions seen in typical IRE procedures. This may also mitigate the likelihood of inducing cardiac arrhythmias and enable treatment without the need for chemical paralytics or cardiac synchronization.

The work presented here indicates that the use of a small number of high energy bursts may be beneficial as statistically equivalent lesion volumes were created by 40–200 bursts when pulse length, number of cycles, and voltage were held constant. Using IRE pulses, Bonakdar *et al.* observed a large change in the conductivity of potato tissue during the first 30 pulses and a significantly less dramatic change between 30 and 100 pulses[55] indicating that most electroporation is occurring early on in the treatment. Typical clinical IRE protocols follow the guidance reported in early studies by Al-Sakere *et al.* for the delivery of 100 pulses per location and some treatment protocols have been reported with 270 total pulses per treatment location.[58] The results reported here indicate that pulse delivery, beyond a critical threshold, may not significantly increase the ablation volume.

This data does not refute the clinical benefit that additional pulses may provide and it is possible that the optimal number of pulses is different for various healthy and tumorous tissue types which cannot be recreated in a potato model. However, further investigation *in vivo* is warranted as this could have significant translational effects through the reduction of operating room time and anesthetic dose required. Additionally, overall procedure costs climb the longer the patient is under anesthesia or in a perioperative state and therefore a systematic reduction in this time is financially beneficial. For example, when treating large tumors (>3 cm), it is common for physicians to bracket the tumor with four or more electrodes and deliver pulses between each probe combination. A hypothetical four electrode treatment would currently deliver 600 pulses. If it is found *in vivo* that ablation volumes do not increase past 40 pulses, than this would reduce the total treatment by 60% to 240 pulses. This has the potential to drastically shorten treatment times for very large tumors where the electrodes are pulled back to treat multiple locations.

There are a number of important limitations to this study. Potato tissue is far from an ideal model for investigating IRE. The lethal thresholds for potato tissue are drastically lower than mammalian tissue resulting in ablations which are substantially larger than those seen *in vivo*. Additionally, this tissue phantom model is not perfused and Joule heating could be greater in this model than observed *in vivo*. It is unclear how lethal thresholds observed in this model will translate to healthy and cancerous tissues *in vivo* and the thresholds presented here should not be used for clinical treatment planning. Despite these limitations, potato remains the one of the most viable

models for comparing the effects of different H-FIRE protocols at clinically relevant voltages (1000–3000 V).

CONCLUSION

In this study, we used a potato tissue phantom model to confirm *in vitro* data on cells in suspension and 3D culture which showed that lethal thresholds for H-FIRE treatments increase as constitutive pulse duration decreases, even when equivalent energy doses are delivered. Data from these studies indicate that delivering over 40 bursts, while holding other parameters constant, does not significantly reduce the threshold for cell death or increase the total ablation volume. This implies that alternative strategies are necessary to increase the size of ablations created by H-FIRE. Future work should focus on optimizing protocols to deliver the fewest high-energy H-FIRE bursts possible while avoiding thermal damage to the tissue.

ELECTRONIC SUPPLEMENTARY MATERIAL

The online version of this article (doi: 10.1007/s10439-017-1889-2) contains supplementary material, which is available to authorized users.

ACKNOWLEDGMENTS

This work was supported in part by the NSF through GRFP, STTR 1346343 and IIP 12655105, the Virginia Center for Innovative Technology (VA-CIT) through MF13-034-LS, the NIH through R21 CA192042-01, and the DOD through the Prostate Cancer Research Program (PCRP) Postdoctoral Training Award W81XWH-15-1-0137. The authors would also like to thank the Virginia Tech Institute for Critical Technologies and Applied Sciences (ICTAS), the Virginia Tech-Knowledge Works, and the Virginia Tech Corporate Research Center (VT-CRC) for their support of this Project.

CONFLICTS OF INTEREST

MBS, ELL, MRD, and RVD have accepted/pending patents on IRE based technologies. All other authors have no conflicts to report.

REFERENCES

[1]Heller, L. C., and R. Heller. In vivo electroporation for gene therapy. *Hum. Gene Ther*. 17:890–897, 2006.

[2]Ivorra, A., L. M. Mir, and B. Rubinsky. Electric field redistribution due to conductivity changes during tissue electroporation: experiments with a simple vegetal model. *IFMBE Proc*. 25:59–62, 2009.

[3]Miklavcic, D., B. Mali, B. Kos, R. Heller, and G. Sersa. Electrochemotherapy: from the drawing board into medical practice. *Biomed. Eng. Online* 2014. doi: 10.1186/1475-925X-13-29.

[4]Yarmush, M. L., A. Golberg, G. Sersa, T. Kotnik, and D. Miklavcic. Electroporation-based technologies for medicine: principles, applications, and challenges. *Annu. Rev. Biomed. Eng*. 16:295–320, 2014.

[5]Jaroszeski, M. J., *et al*. Toxicity of anticancer agents mediated by electroporation in vitro. *Anti-cancer Drug* 11:201–208, 2000.

[6]Dean, D. A. Nonviral gene transfer to skeletal, smooth, and cardiac muscle in living animals. *Am. J. Physiol. Cell Physiol*. 289:C233–C245, 2005.

[7]Davalos, R. V., L. M. Mir, and B. Rubinsky. Tissue ablation with irreversible electroporation. *Ann. Biomed. Eng*. 33:223–231, 2005.

[8]Jiang, C. L., R. V. Davalos, and J. C. Bischof. A review of basic to clinical studies of irreversible electroporation therapy. *IEEE Trans. Biomed. Eng*. 62:4–20, 2015.

[9]Chu, K. F., and D. E. Dupuy. Thermal ablation of tumours: biological mechanisms and advances in therapy. *Nat. Rev. Cancer* 14:199–208, 2014.

[10]Siddiqui, I. A., *et al*. High-frequency irreversible electroporation: safety and efficacy of next-generation irreversible electroporation adjacent to critical hepatic structures. *Surg. Innov*. 2017. doi:10.1177/1553350617692202.

[11]Scheffer, H. J., *et al*. Irreversible electroporation for nonthermal tumor ablation in the clinical setting: a systematic review of safety and efficacy. *J. Vasc. Interv. Radiol*. 25:997–1011, 2014.

[12]Garcia, P. A., *et al*. Non-thermal irreversible electroporation (N-TIRE) and adjuvant fractionated radiotherapeutic multimodal therapy for intracranial malignant glioma in a canine patient. *Technol. Cancer Res. Treat*. 10:73–83, 2011.

[13]Garcia, P. A., J. H. Rossmeisl Jr., T. L. Ellis, and R. V. Davalos. Nonthermal irreversible electroporation as a focal ablation treatment for brain cancer. In: Tumors of the Central Nervous System, Volume 12. Dordrecht: Springer, pp. 171–182, 2014.

[14]Martin, R. C., E. Schwartz, J. Adams, I. Farah, and B. M. Derhake. Intra-operative anesthesia management in patients undergoing surgical irreversible electroporation of the pancreas, liver, kidney, and retroperitoneal tumors. *Anesthesiol. Pain Med*. 5:e22786, 2015.

[15]Bower, M., L. Sherwood, Y. Li, and R. Martin. Irreversible electroporation of the pancreas: definitive local therapy without systemic effects. *J. Surg. Oncol*. 104:22–28, 2011.

[16]Scheffer, H. J., *et al*. Irreversible electroporation for nonthermal tumor ablation in the clinical setting: a systematic review of safety and efficacy. *J. Vasc. Interv. Radiol*. 2014. doi:10.1016/j.jvir.2014.01.028.

[17]Cheung, W., *et al*. Irreversible electroporation for unresectable hepatocellular carcinoma: initial experience and review of safety and outcomes. *Technol. Cancer Res. Treat*. 12:233, 2013.

[18]Cannon, R., S. Ellis, D. Hayes, G. Narayanan, and R. C. Martin. Safety and early efficacy of irreversible electroporation for hepatic tumors in proximity to vital structures. *J. Surg. Oncol*. 107:544–549, 2013.

[19]Martin, II, R. C., K. McFarland, S. Ellis, and V. Velanovich. Irreversible electroporation in locally advanced pan-

creatic cancer: potential improved overall survival. *Ann. Surg. Oncol.* 20:443–449, 2013.
[20]Martin, II, R. C., K. McFarland, S. Ellis, and V. Velanovich. Irreversible electroporation therapy in the management of locally advanced pancreatic adenocarcinoma. *J. Am. Coll. Surg.* 215:361–369, 2012.
[21]Usman, M., W. Moore, R. Talati, K. Watkins, and T. V. Bilfinger. Irreversible electroporation of lung neoplasm: a case series. *Med. Sci. Monit. Int. Med. J. Exp. Clin. Res.* 18:CS43, 2012.
[22]Garcia, P. A., *et al.* Intracranial nonthermal irreversible electroporation: in vivo analysis. *J. Membr. Biol.* 236:127–136, 2010.
[23]Pech, M., *et al.* Irreversible electroporation of renal cell carcinoma: a first-in-man phase I clinical study. *Cardiovasc. Interv. Radiol.* 34:132–138, 2011.
[24]Wendler, J. J., *et al.* Angiography in the isolated perfused kidney: radiological evaluation of vascular protection in tissue ablation by nonthermal irreversible electroporation. *Cardiovasc. Interv. Radiol.* 35:383–390, 2012.
[25]Wendler, J. J., *et al.* Urinary tract effects after multifocal nonthermal irreversible electroporation of the kidney: acute and chronic monitoring by magnetic resonance imaging, intravenous urography and urinary cytology. *Cardiovasc. Interv. Radiol.* 35:921–926, 2012.
[26]Wendler, J., *et al.* Short- and mid-term effects of irreversible electroporation on normal renal tissue: an animal model. *Cardiovasc. Interv. Radiol.* 36:512–520, 2013.
[27]Olweny, E. O., *et al.* Irreversible electroporation: evaluation of nonthermal and thermal ablative capabilities in the porcine kidney. *Urology* 81:679–684, 2013.
[28]Kingham, T. P., *et al.* Ablation of perivascular hepatic malignant tumors with irreversible electroporation. *J. Am. Coll. Surg.* 215:379–387, 2012.
[29]Charpentier, K. P. Irreversible electroporation for the ablation of liver tumors: are we there yet? *Arch. Surg.* 147:1053–1061, 2012.
[30]Lee, E. W., C. T. Loh, and S. T. Kee. Imaging guided percutaneous irreversible electroporation: ultrasound and immunohistological correlation. *Technol. Cancer Res. Treat.* 6:287–293, 2007.
[31]Rubinsky, B., G. Onik, and P. Mikus. Irreversible electroporation: a new ablation modality—clinical implications. *Technol. Cancer Res. Treat.* 6:37–48, 2007.
[32]Lee, E. W., *et al.* Advanced hepatic ablation technique for creating complete cell death: irreversible electroporation. *Radiology* 255:426–433, 2010.
[33]Ricke, J., *et al.* Irreversible electroporation (IRE) fails to demonstrate efficacy in a prospective multicenter phase II trial on lung malignancies: The ALICE trial. *Cardiovasc. Interv. Radiol.* 38:401–408, 2015.
[34]Daniels, C., and B. Rubinsky. Electrical field and temperature model of nonthermal irreversible electroporation in heterogeneous tissues. *J. Biomech. Eng. Trans. ASME* 2009. doi:10.1115/1.3156808.
[35]Arena, C. B., M. B. Sano, M. N. Rylander, and R. V. Davalos. Theoretical considerations of tissue electroporation with high-frequency bipolar pulses. *IEEE Trans. Biomed. Eng.* 58:1474–1482, 2011.
[36]Golberg, A., B. G. Bruinsma, B. E. Uygun, and M. L. Yarmush. Tissue heterogeneity in structure and conductivity contribute to cell survival during irreversible electroporation ablation by "electric field sinks". *Sci. Rep.* 5:8485, 2015.
[37]Gabriel, S., R. Lau, and C. Gabriel. The dielectric properties of biological tissues: II. Measurements in the frequency range 10 Hz to 20 GHz. *Phys. Med. Biol.* 41:2251, 1996.
[38]Bhonsle, S. P., C. B. Arena, D. C. Sweeney, and R. V. Davalos. Mitigation of impedance changes due to electroporation therapy using bursts of high-frequency bipolar pulses. *Biomed. Eng. Online* 2015. doi:10.1186/1475-925X-14-S3-S3.
[39]Arena, C. B., *et al.* High-frequency irreversible electroporation (H-FIRE) for non-thermal ablation without muscle contraction. *Biomed. Eng. Online* 2011. doi:10.1186/1475-925X-10-102.
[40]Weaver, J. C., K. C. Smith, A. T. Esser, R. S. Son, and T. Gowrishankar. A brief overview of electroporation pulse strength-duration space: a region where additional intracellular effects are expected. *Bioelectrochemistry* 2012. doi:10.1016/j.bioelechem.2012.02.007.
[41]Sano, M. B., C. B. Arena, M. R. DeWitt, D. Saur, and R. V. Davalos. In-vitro bipolar nano- and microsecond electro-pulse bursts for irreversible electroporation therapies. *Bioelectrochemistry* 100:69–79, 2014.
[42]Kotnik, T., and D. Miklavčič. Theoretical evaluation of voltage inducement on internal membranes of biological cells exposed to electric fields. *Biophys. J.* 90:480–491, 2006.
[43]Tsong, T. Y. On electroporation of cell membranes and some related phenomena. *J. Electroanal. Chem. Interfacial Electrochem.* 299:271–295, 1990.
[44]Arena, C. B., C. S. Szot, P. A. Garcia, M. N. Rylander, and R. V. Davalos. A three-dimensional in vitro tumor platform for modeling therapeutic irreversible electroporation. *Biophys. J.* 103:2033–2042, 2012.
[45]Sano, M. B., *et al.* Bursts of bipolar microsecond pulses inhibit tumor growth. *Sci. Rep.* 2015. doi:10.1038/srep14999.
[46]Sano, M. B., *et al.* Towards the creation of decellularized organ constructs using irreversible electroporation and active mechanical perfusion. *Biomed. Eng. Online* 9:83, 2010.
[47]Edd, J. F., L. Horowitz, R. V. Davalos, L. M. Mir, and B. Rubinsky. In vivo results of a new focal tissue ablation technique: irreversible electroporation. *IEEE Trans. Biomed. Eng.* 53:1409–1415, 2006.
[48]Miklavčič, D., D. Šemrov, H. Mekid, and L. M. Mir. A validated model of in vivo electric field distribution in tissues for electrochemotherapy and for DNA electrotransfer for gene therapy. *Biochim. Biophys. Acta Gen. Subj.* 1523: 73–83, 2000.
[49]Hjouj, M., and B. Rubinsky. Magnetic resonance imaging characteristics of nonthermal irreversible electroporation in vegetable tissue. *J. Membr. Biol.* 236:137–146, 2010.
[50]Neal, R. E., *et al.* In vivo irreversible electroporation kidney ablation: experimentally correlated numerical models. *IEEE Trans. Biomed. Eng.* 62:561–569, 2015.
[51]Neal, R. E., *et al.* In vivo characterization and numerical simulation of prostate properties for non-thermal irreversible electroporation ablation. *Prostate* 74:458–468, 2014.
[52]Makower, R., and S. Schwimmer. Inhibition of enzymic color formation in potato by adenosine triphosphate. *Biochem. Biophys. Acta* 14:156–157, 1954.
[53]Ivorra, A., L. Mir, and B. Rubinsky. Electric field redistribution due to conductivity changes during tissue electroporation: experiments with a simple vegetal model. In: World Congress on Medical Physics and Biomedical Engineering, 7–12 September 2009, Munich, Germany. Berlin: Springer, 2010, pp. 59–62.
[54]Edd, J. F., and R. V. Davalos. Mathematical modeling of irreversible electroporation for treatment planning. *Technol. Cancer Res. Treat.* 6:275–286, 2007.

[55]Bonakdar, M., E. L. Latouche, R. L. Mahajan, and R. V. Davalos. The feasibility of a smart surgical probe for verification of IRE treatments using electrical impedance spectroscopy. *IEEE Trans. Biomed. Eng*. 62:2674–2684, 2015.

[56]Yao, C., *et al*. Bipolar microsecond pulses and insulated needle electrodes for reducing muscle contractions during irreversible electroporation. *IEEE Trans. Biomed. Eng*. 2017. doi:10.1109/TBME.2017.2690624.

[57]Deodhar, A., *et al*. Irreversible electroporation near the heart: ventricular arrhythmias can be prevented with ECG synchronization. *Am. J. Roentgenol*. 196:W330–W335, 2011.

[58]Dunki-Jacobs, E., P. Philips, and I. Martin. Evaluation of thermal injury to liver, pancreas and kidney during irreversible electroporation in an in vivo experimental model. *Br. J. Surg*. 101:1113–1121, 2014.